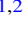




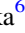




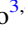

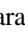
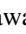






CrossMark

Cerium Features in Kilonova Near-infrared Spectra: Implication from a Chemically Peculiar Star

Masaomi Tanaka^{1,2} , Nanae Domoto¹ , Wako Aoki^{3,4} , Miho N. Ishigaki³ , Shinya Wanajo⁵ , Kenta Hotokezaka^{6,7} ,
Kyohei Kawaguchi^{5,8,9} , Daiji Kato^{10,11} , Jae-Joon Lee¹² , Ho-Gyu Lee^{12,13} , Teruyuki Hirano^{3,4,14} ,
Takayuki Kotani^{3,4,14} , Masayuki Kuzuhara^{3,14} , Jun Nishikawa^{3,4,14} , Masashi Omiya^{3,14} , Motohide Tamura^{3,14,15} , and
Akitoshi Ueda^{3,4,14}

¹ Astronomical Institute, Tohoku University, Aoba, Sendai 980-8578, Japan; masaomi.tanaka@astr.tohoku.ac.jp

² Division for the Establishment of Frontier Sciences, Organization for Advanced Studies, Tohoku University, Sendai 980-8577, Japan

³ National Astronomical Observatory of Japan, 2-21-1 Osawa, Mitaka, Tokyo 181-8588, Japan

⁴ Astronomical Science Program, The Graduate University for Advanced Studies, SOKENDAI, 2-21-1 Osawa, Mitaka, Tokyo 181-8588, Japan

⁵ Max-Planck-Institut für Gravitationsphysik (Albert-Einstein-Institut), Am Mühlenberg 1, D-14476 Potsdam-Golm, Germany

⁶ Research Center for the Early Universe, Graduate School of Science, University of Tokyo, Bunkyo, Tokyo 113-0033, Japan

⁷ Kavli IPMU (WPI), UTIAS, The University of Tokyo, Kashiwa, Chiba 277-8583, Japan

⁸ Institute for Cosmic Ray Research, The University of Tokyo, Kashiwa, Chiba 277-8582, Japan

⁹ Center for Gravitational Physics, Yukawa Institute for Theoretical Physics, Kyoto University, Kyoto 606-8502, Japan

¹⁰ National Institute for Fusion Science, 322-6 Oroshi-cho, Toki 509-5292, Japan

¹¹ Interdisciplinary Graduate School of Engineering Sciences, Kyushu University, Kasuga, Fukuoka 816-8580, Japan

¹² Korea Astronomy and Space Science Institute, 776 Daedeok-daero, Yuseong-gu, Daejeon 34055, Republic of Korea

¹³ Space Policy Research Center, Science and Technology Policy Institute, 370 Sicheong-daero, Sejong 30147, Republic of Korea

¹⁴ Astrobiology Center, 2-21-1 Osawa, Mitaka, Tokyo 181-8588, Japan

¹⁵ Department of Astronomy, Graduate School of Science, The University of Tokyo, 7-3-1 Hongo, Bunkyo-ku, Tokyo 113-0033, Japan

Received 2023 April 16; revised 2023 May 25; accepted 2023 June 6; published 2023 July 28

Abstract

Observations of the kilonova from the neutron star merger event GW170817 opened a way to study *r*-process nucleosynthesis directly using neutron star mergers. It is, however, challenging to identify individual elements in kilonova spectra due to a lack of complete atomic data, in particular at near-infrared (NIR) wavelengths. In this paper, we demonstrate that spectra of chemically peculiar stars with enhanced heavy-element abundances can provide us with an excellent astrophysical laboratory for kilonova spectra. We show that the photosphere of the late B-type, chemically peculiar star HR 465 has similar lanthanide abundances and ionization degrees with those in the line-forming region in a kilonova at ~ 2.5 days after the merger. The NIR spectrum of HR 465 taken with Subaru/IRD indicates that Ce III lines give the strongest absorption feature around 16000 Å and there are no other comparably strong transitions around these lines. The Ce III lines nicely match with the broad absorption feature at 14500 Å observed in GW170817 with a blueshift of $v = 0.1 c$, which supports recent identification of this feature as Ce III by Domoto et al.

Unified Astronomy Thesaurus concepts: Neutron stars (1108); R-process (1324); Transient sources (1851); Stellar spectral lines (1630)

1. Introduction

Multimessenger observations of the neutron star merger GW170817 opened a new pathway to study the astrophysical sites of *r*-process nucleosynthesis. Following the detection of gravitational waves, an electromagnetic counterpart was identified in ultraviolet, optical, and infrared wavelengths (AT 2017gfo; Abbott et al. 2017). The properties of AT 2017gfo are consistent with those of a kilonova (e.g., Li & Paczyński 1998; Metzger et al. 2010), a thermal emission powered by the decay of *r*-process nuclei, which gives evidence that neutron star mergers are a site of *r*-process nucleosynthesis (e.g., Kasen et al. 2017; Perego et al. 2017; Tanaka et al. 2017; Kawaguchi et al. 2018; Rosswog et al. 2018).

To extract detailed information of *r*-process nucleosynthesis, such as the amounts of individual elements and their spatial distribution, it is necessary to identify elements in spectra as done for stellar spectra. In fact, a series of optical and near-infrared (NIR) spectra

have been taken for AT 2017gfo (e.g., Chornock et al. 2017; Pian et al. 2017; Smartt et al. 2017). However, it is challenging to decode the spectra due to high Doppler shifts of the spectral lines, the presence of many heavy elements, and a lack of complete and accurate atomic data, in particular, at NIR wavelengths.

Watson et al. (2019) proposed that the observed absorption features around 9000 Å are caused by Sr II lines. This identification was further confirmed by Domoto et al. (2021) with full radiative transfer simulations. Also, Gillanders et al. (2022) quantified the Sr abundance by atmospheric modeling. The same feature may also be caused by a He I line (Perego et al. 2022), although the strength of the He I line depends on non-local thermodynamic equilibrium (non-LTE) effects (Tarumi et al. 2023).

Recently, Domoto et al. (2022) systematically studied the spectral features of kilonovae at NIR wavelengths. They identified several elements producing strong transitions in kilonovae, such as Ca, Sr, Y, Zr, Ba, La, and Ce. Then, they constructed a hybrid line list by combining a theoretical line list based on atomic models of Tanaka et al. (2020) and an accurate line list of the important ions based on spectroscopic experiments. By performing radiative transfer simulations with the hybrid line list, they showed that the broad NIR features



Original content from this work may be used under the terms of the [Creative Commons Attribution 4.0 licence](https://creativecommons.org/licenses/by/4.0/). Any further distribution of this work must maintain attribution to the author(s) and the title of the work, journal citation and DOI.

around 13000 Å and 14500 Å in AT 2017gfo are reproduced by La III and Ce III lines, respectively.

There are, however, still no complete and accurate atomic data at NIR wavelengths, which cover all the heavy elements synthesized in neutron star mergers. Therefore, there might be unknown transitions of other elements that contribute to the NIR absorption features of kilonova spectra.

In this paper, we demonstrate that the atmospheres of chemically peculiar stars provide an excellent laboratory to decode kilonova spectra. Chemically peculiar stars are known to exhibit abnormal elemental abundance patterns. Some chemically peculiar stars show extremely enhanced metal abundances (hereafter we call stars with enhanced metal abundances as chemically peculiar stars), which are likely to be caused by atomic diffusion (Michaud 1970). Thus, the atmospheres of such stars can mimic the elemental abundances in kilonovae dominated by heavy elements. In Section 2, we show similarities in the atmospheres of chemically peculiar stars and kilonovae by analyzing the properties of the late B-type chemically peculiar star HR 465 (HD 9996; e.g., Preston & Wolff 1970; Aller 1972; Cowley & Greenberg 1987). In Section 3, we show an NIR spectrum of HR 465 and measurements of strong absorption lines. Then, we discuss implications to kilonova spectra in Section 4. Finally we give concluding remarks in Section 5. All the wavelengths given in this paper are those in air.

2. A Chemically Peculiar Star as a Laboratory for Kilonova Spectra

2.1. Abundances

Abundances in the ejected material from neutron star mergers (hereafter kilonova ejecta) are dominated by elements heavier than Fe. The top panel of Figure 1 shows an abundance distribution adopted in the radiative transfer simulations by Domoto et al. (2021) and Domoto et al. (2022) as a representative case of kilonova ejecta (their “light” model that assumes a solar r -process-like pattern with an enhanced light component; see also Wanajo 2018). This particular example is a case that is consistent with the abundances of metal-poor stars with a weak r -process signature such as HD 122563 (Honda et al. 2006).

Chemically peculiar stars often show enhanced abundances of elements heavier than Fe (e.g., Ghazaryan et al. 2018). In particular, Ap- and Bp-type stars show the abundances of lanthanides (atomic number $Z = 57-71$) enhanced by more than two orders of magnitude, which can match the high heavy-element abundances in kilonovae. The red points in Figure 1 (top panel) show the elemental abundances of HR 465 (B9p; Nielsen et al. 2020). HR 465 is an intensively studied chemically peculiar star (e.g., Preston & Wolff 1970; Aller 1972; Cowley & Greenberg 1987) with a metallicity of $[\text{Fe}/\text{H}] \simeq +1.0$ (Nielsen et al. 2020). As clearly shown in Figure 1 (top panel), the abundances of heavy elements in HR 465 are greatly enhanced as compared with the solar abundance pattern (black; Asplund et al. 2009).¹⁶

¹⁶ The abundances of HR 465 are known to evolve with photometric/magnetic phase (Rice 1988) with a period of 21.5 yr (Pyper & Adelman 2017). The abundances of the rare-earth elements reach a maximum at $\phi \simeq 0$ and minimum at $\phi \simeq 0.5$. Our Subaru InfraRed Doppler (IRD) observations (Section 3) are performed at $\phi = 0.77$. We show the abundances in Figure 1 by taking the averages of the abundances derived from the lines of different ionization degrees (if any) at different phases ($\phi = 0.45, 0.68, \text{ and } 0.85$; Nielsen et al. 2020). The variation is up to about one order of magnitude, and the global trend discussed in this paper is not affected.

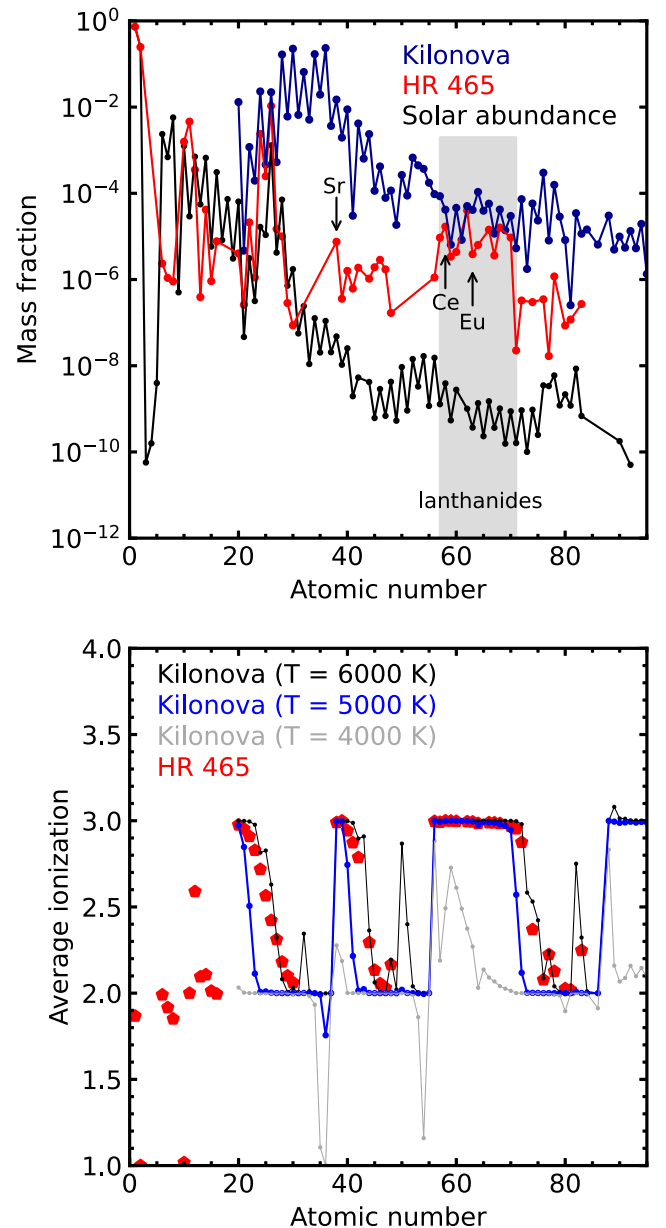


Figure 1. Top: abundances in kilonova ejecta at $t = 2.5$ days (blue; Domoto et al. 2021, 2022) compared with those of the chemically peculiar star HR 465 (red; Nielsen et al. 2020) and solar abundances (black). Bottom: average ionization degrees in the photospheres of kilonovae (black, blue, and gray lines) and HR 465 (red) calculated under the assumption of LTE.

In particular, the abundances of lanthanides ($Z = 57-71$) in HR 465 are enhanced by about three orders of magnitude, and their mass fractions are remarkably similar to those in the kilonova ejecta. Lanthanides are known to produce strong lines at NIR wavelengths due to their low-lying, dense energy levels (Kasen et al. 2013; Tanaka & Hotokezaka 2013; Fontes et al. 2020). Thus, thanks to the similarities in the abundances, the NIR spectra of such chemically peculiar stars can provide candidates for the strong absorption lines of lanthanides in kilonova NIR spectra.

2.2. Ionization Degrees

Some chemically peculiar stars also have similar ionization degrees with those in kilonova ejecta a few days after the

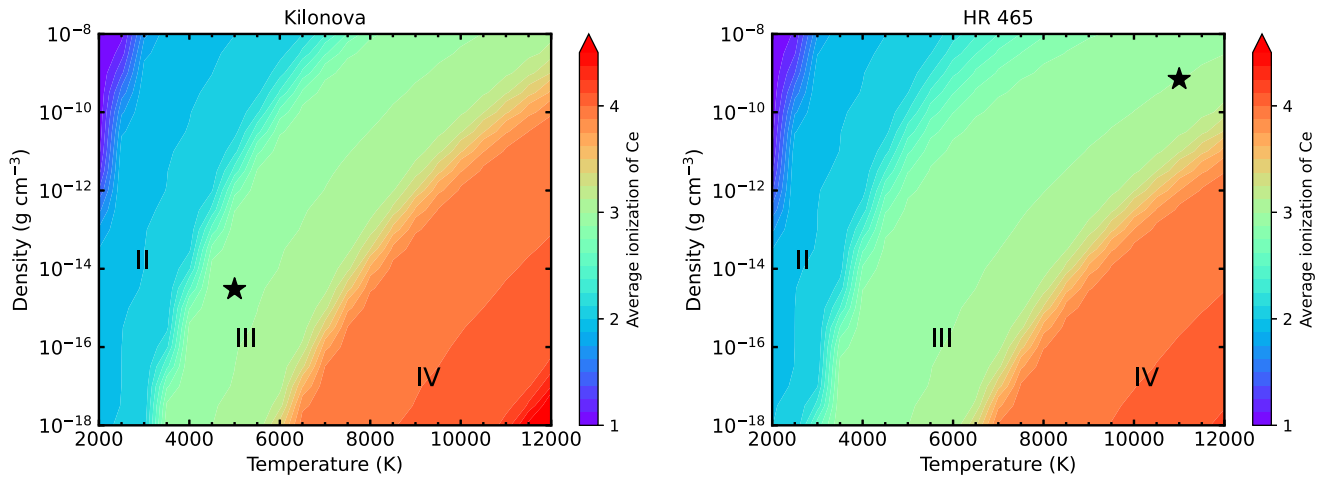


Figure 2. Left: average ionization degree of Ce as a function of temperature and density for the abundances of kilonovae (blue points in the top panel of Figure 1). Right: the same for the abundances of HR 465 (red points in the top panel of Figure 1). The fiducial parameters for the kilonova ejecta and the photosphere of HR 465 are marked with star symbols. The boundary between the doubly (III) and triply (IV) ionized regions is different between the two cases. This is because of the H-rich abundances in HR 465, where the free electrons are mainly provided by ionized H at a high temperature.

merger. The bottom panel of Figure 1 compares the ionization degrees of kilonova with those of HR 465. The lines show average ionization degrees (neutral is denoted as 1, single ionization is denoted as 2, and so on) in the line-forming region in a kilonova calculated under the assumption of LTE. The fiducial case (blue line) is calculated by assuming the abundance distribution as in the top panel, with a temperature of $T = 5000$ K and a matter density of $\rho = 3 \times 10^{-15} \text{ g cm}^{-3}$. These parameters are chosen based on the properties of the line-forming region at the NIR wavelength ($v = 0.1 c$) at $t = 2.5$ days after the merger in the radiative transfer simulations (see Figure 6 of Domoto et al. 2022). Typically, heavy elements are singly or doubly ionized under these conditions, and most of the lanthanides are doubly ionized.

The temperature assumed here is somewhat higher than those derived by blackbody fitting to the observed kilonova spectra ($T \sim 4000$ K; e.g., Watson et al. 2019; Sneppen et al. 2023). The difference stems from the fact that the line-forming region in the NIR lines is located at an inner layer ($v \sim 0.1 c$) rather than the “photospheric” velocity of $v \sim 0.25 c$) due to the lower opacities at the NIR wavelengths (Tanaka et al. 2020). To see the dependence of the ionization on the temperature, we also show the ionization degrees at $T = 6000$ K (black line in the bottom panel of Figure 1) and $T = 4000$ K (gray line). Also, the left panel of Figure 2 shows the average ionization of Ce for a wide range of temperatures and densities. Under the LTE assumption, the ionization degrees in kilonova ejecta depend on the temperature rather strongly around $T = 5000$ K. For example, the latter half of the lanthanides become singly ionized at $T = 4000$ K (gray line in the bottom panel of Figure 1). Note that, as we neglect ionization by nonthermal electrons produced by the beta decay of radioactive nuclei, the ionization degrees tend to be underestimated (see also Section 5).

The dominance of doubly ionized lanthanides is also seen in late B-type or early A-type dwarf stars with an effective temperature of $T_{\text{eff}} \sim 10,000$ K. The red points in the bottom panel of Figure 1 show the average ionization degrees at the photosphere of HR 465 for $T = 11,000$ K and $\rho = 7 \times 10^{-10} \text{ g cm}^{-3}$. These parameters are taken based on the ATLAS9 atmospheric model (Castelli & Kurucz 2003) with

the stellar parameters of HR 465 ($\log g = 4.0$ and $T_{\text{eff}} = 11,000$ K), a microturbulence velocity of 2 km s^{-1} , and a metallicity of $[M/H] = 0.5$, which is the most metal-rich model available.¹⁷ For the calculation of ionization, we only include elements with measured abundances. But this does not affect the ionization degrees because most of the free electrons are provided by H and Fe.

Although the photospheric temperature of HR 465 is higher than the temperature in the line-forming region of kilonovae at $t = 2.5$ days, the ionization degrees are similar in these two cases. This behavior is highlighted in Figure 2. For a given temperature, the ionization degrees decrease at higher densities. Thus, the higher matter density and higher temperature in the stellar photosphere result in a similar ionization degree with those in kilonovae. Around the parameter space of HR 465, the ionization degrees are not very sensitive to the temperature: doubly ionized lanthanides are still dominant even with $T = 11,000 \pm 1000$ K.

In summary, the photosphere of late B-type or early A-type dwarf stars show similar ionization degrees with those of the line-forming regions of kilonovae at early phases. The photospheres of chemically peculiar stars have a higher temperature than those in kilonovae, and thus, for a given ion, more lines can become active in the photosphere of chemically peculiar stars. Therefore, the spectra of these stars can provide a complete and accurate line list for strong transitions of the elements with a similar abundance in kilonovae (i.e., lanthanides for the case of HR 465).

3. NIR Spectrum of HR 465

We obtained an NIR high-resolution spectrum of HR 465 using the Subaru Telescope IRD instrument (Tamura et al. 2012; Kotani et al. 2018) on 2020 July 25 (UT) with an exposure time of 300 s. The spectrum covers the wavelength range from 9300 to 17600 Å with a spectral resolution of $R \sim 70,000$. The signal-to-noise ratios of the data range from 150 to 230 per pixel in the one-dimensional spectrum depending on the position of the blaze profiles of the echelle spectrum. This quality is sufficient for the purpose of the

¹⁷ <https://wwwuser.oats.inaf.it/castelli/grids.html>

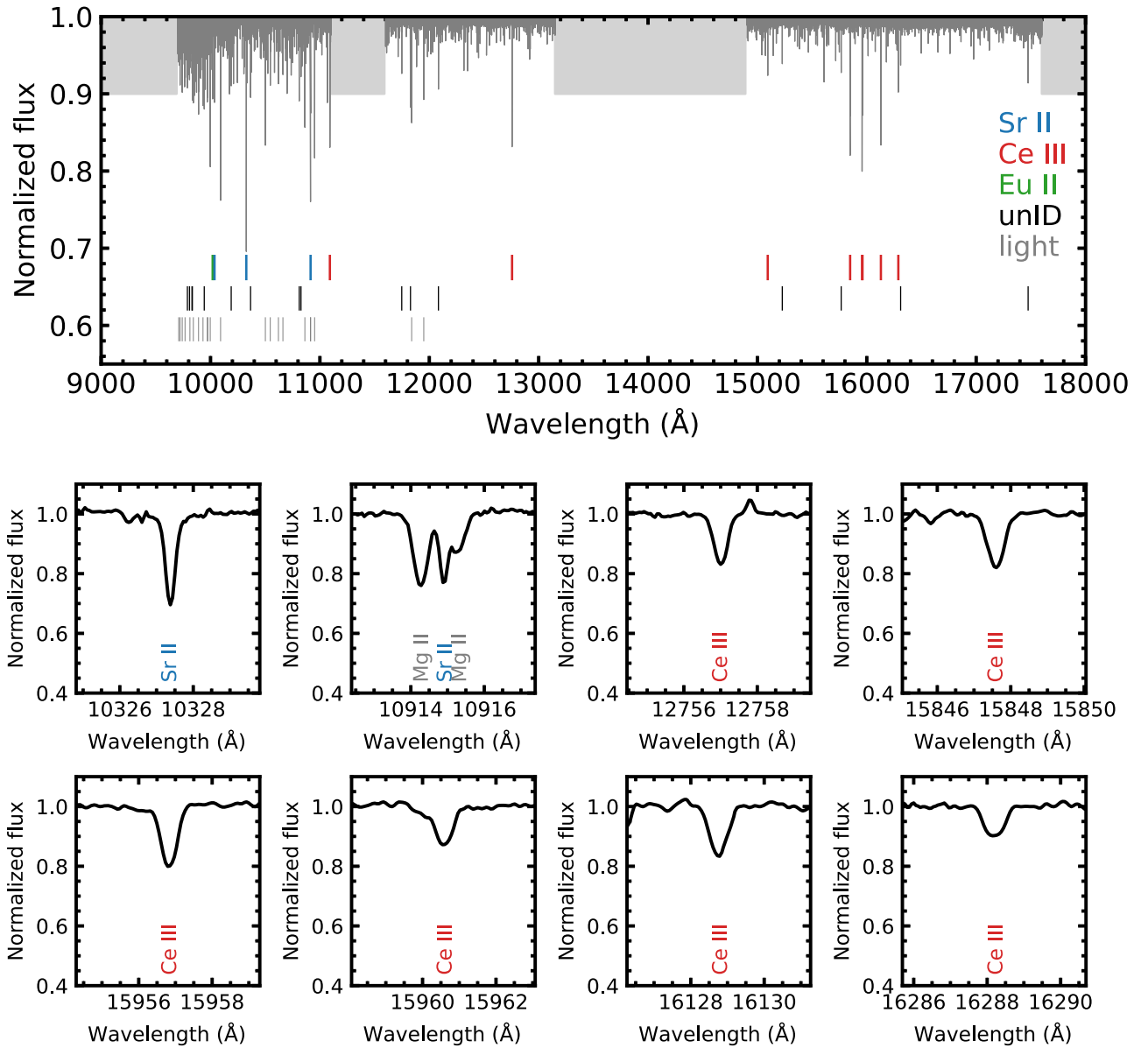


Figure 3. Normalized NIR spectrum of HR 465 (top) and that around the eight strongest transitions of heavy elements (bottom). In the top panel, the 50 strongest lines are indicated. The lines of Sr II, Ce III, and Eu II are shown in red, blue, and green, respectively. The lines of elements lighter than Fe are shown in gray. The lines shown in black are not matched with the line lists (unID). The gray shaded regions show the wavelength ranges with strong atmospheric absorption.

present study. To our knowledge, this is the first high-resolution spectrum of HR 465 covering such a wide NIR wavelength range. The details of the observations and data reduction are reported by Aoki et al. (2022). The telluric absorption lines are correlated by the spectrum of the bright extremely metal-poor star BD+44°493, in which few absorption lines are found in this wavelength range (Aoki et al. 2022).

The top panel of Figure 3 shows the entire spectrum of HR 465 (see Figure 6 for an extended view). The spectrum is normalized by continuum fitting for the ease of line identification. Furthermore, the broad hydrogen absorption features are fitted and the spectrum around those features is flattened. After masking the wavelength ranges with strong atmospheric absorption, i.e., the ranges between the *Y*, *J*, and *H* bands, as well as artifacts from the telluric correction (gray shaded regions without line identifications in Figure 6), we detect strong absorption lines. Then, the detected lines are matched with the VALD line list (Kupka et al. 1999) and the NIR line

list by Domoto et al. (2022). There are some lines with which no known transition is matched, in particular, at shorter wavelengths where more absorption lines exist. We keep these lines as “unID” as they may be caused by heavy elements. Then, we measure the equivalent widths (EWs) of the strong lines by assuming a Gaussian profile.

Figure 4 shows the EWs for the 50 strongest transitions. It is clearly seen that, excluding elements lighter than Fe, the strongest absorptions in the NIR spectrum of HR 465 are dominated by the lines of Ce III and Sr II. The bottom panels of Figure 3 show the spectra around the six strongest transitions of Ce III and two strongest transitions of Sr II.

4. Implications to Kilonova Spectra

We apply the knowledge from HR 465 to the kilonova spectra. In Figure 5, we show the spectrum of HR 465 (top panel) and the EWs of the 50 strongest transitions (bottom

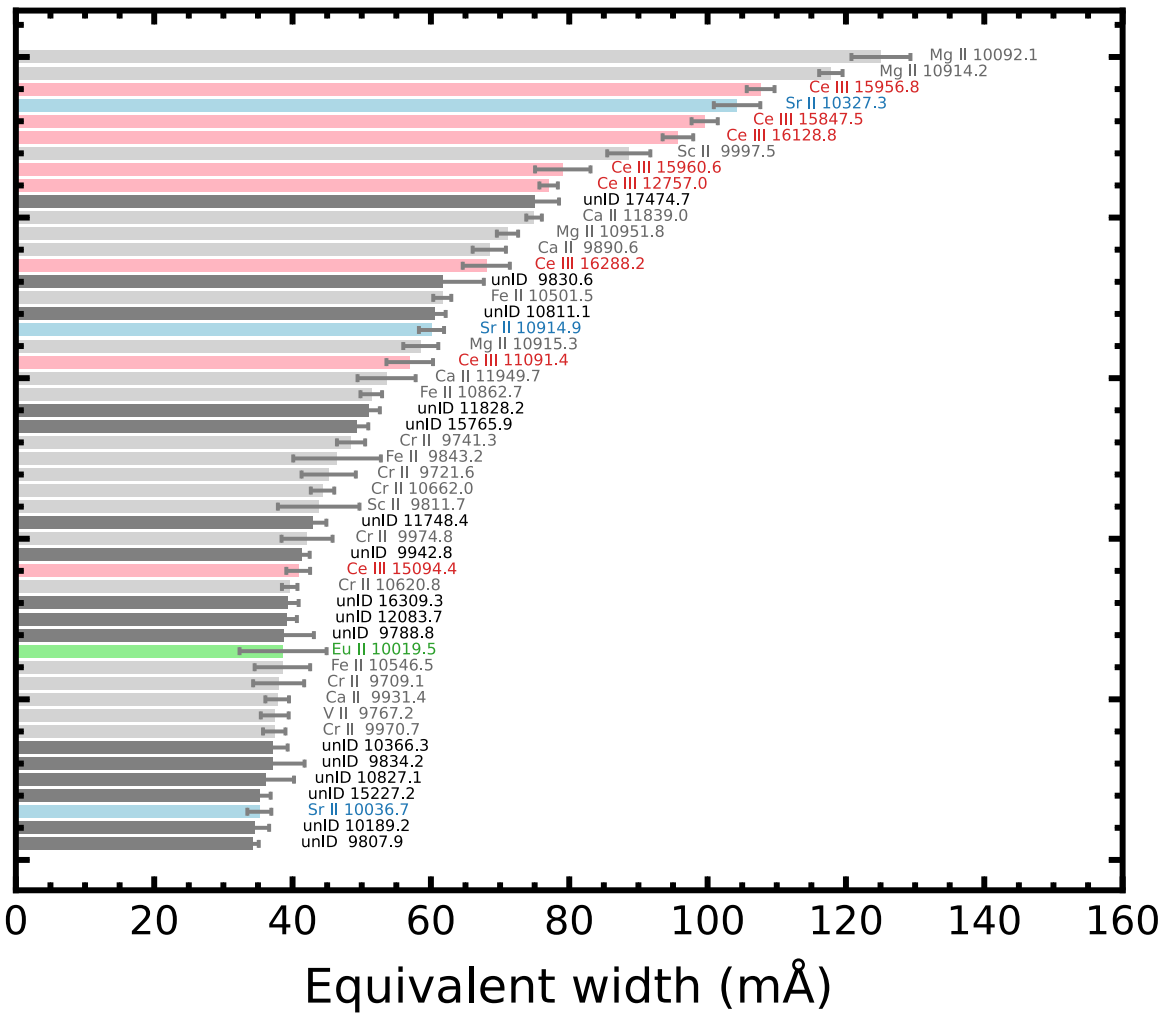


Figure 4. EWs of the 50 strongest lines in the NIR spectrum of HR 465. The lines of elements heavier than Fe, which are abundant in kilonova ejecta, are shown in red (Ce), blue (Sr), and green (Eu), while the lines of lighter elements are shown in gray. The unID lines that can also potentially appear in kilonova spectra are shown in black.

panel) compared with the spectra of AT 2017gfo (Pian et al. 2017; Smartt et al. 2017; Tanvir et al. 2017). To account for the expansion velocity of the ejecta, the lines are blueshifted with a velocity of $v = 0.1 c$. This is a typical velocity of a line-forming region at NIR wavelengths at $t = 2.5$ days in the model of Domoto et al. (2022).

The absorption features of AT 2017gfo around 14500 \AA nicely match with the four strong lines of Ce III (Ce III 15956.8 \AA , 15847.5 \AA , 16128.8 \AA , and 15960.6 \AA) with a blueshift of $v = 0.1 c$ (red lines). Importantly, there are no other elements that cause as strong contributions as Ce III to this feature. These facts support the element identification by Domoto et al. (2022).

The fact that the temperature of HR 465 is higher than in kilonovae makes our findings more indicative. Due to the higher temperature, the excited states of ions are more populated in HR 465, and transitions from a higher excitation energy can become active, which tend to give more candidate ions/transitions when compared with kilonovae. However, the lines corresponding to the 14500 \AA feature are still dominated by Ce III lines, and this further supports our identification of the Ce III lines. Note that the excitation energy of the four strongest transitions of Ce III are $E = 0.0 \text{ eV}$ (ground state), 0.19 eV , 0.39 eV , and 0.81 eV for the Ce III 15956.8 \AA , 15847.5 \AA ,

16128.8 \AA , and 15960.6 \AA lines, respectively. Thus, the lower states of these transitions are well populated even at the temperature of kilonova ejecta ($T \sim 5000 \text{ K}$).

It is worth noting that HR 465 also shows the strong Ce III 12757.0 \AA line, which is a transition from the ground state. Since this line is as strong as those around 16000 \AA and relatively isolated, it may also contribute to the kilonova spectra. Interestingly, there is a hint of a weak trough around 11500 \AA in the HST spectrum of AT 2017gfo (Tanvir et al. 2017). If this tentative identification is tested by high-quality, time-series spectra of kilonovae detected in the future, it strengthens the identification of the Ce III lines in the NIR wavelength range.

Also, the absorption features around 9000 \AA match with the Sr II lines. Note that the velocity of the line-forming region depends on wavelength due to the wavelength dependence of the opacity: the line-forming region is located at higher velocities at optical wavelengths due to the higher optical opacity. A velocity of $v \sim 0.2 c$ is more consistent with the observed features in AT 2017gfo as also demonstrated by Watson et al. (2019). As the Sr abundances are quite different between HR 465 and kilonovae (top panel of Figure 1) and the lower levels of these Sr II lines have a relatively high excitation energy ($E = 1.8 \text{ eV}$), the relative line strengths in HR 465 do

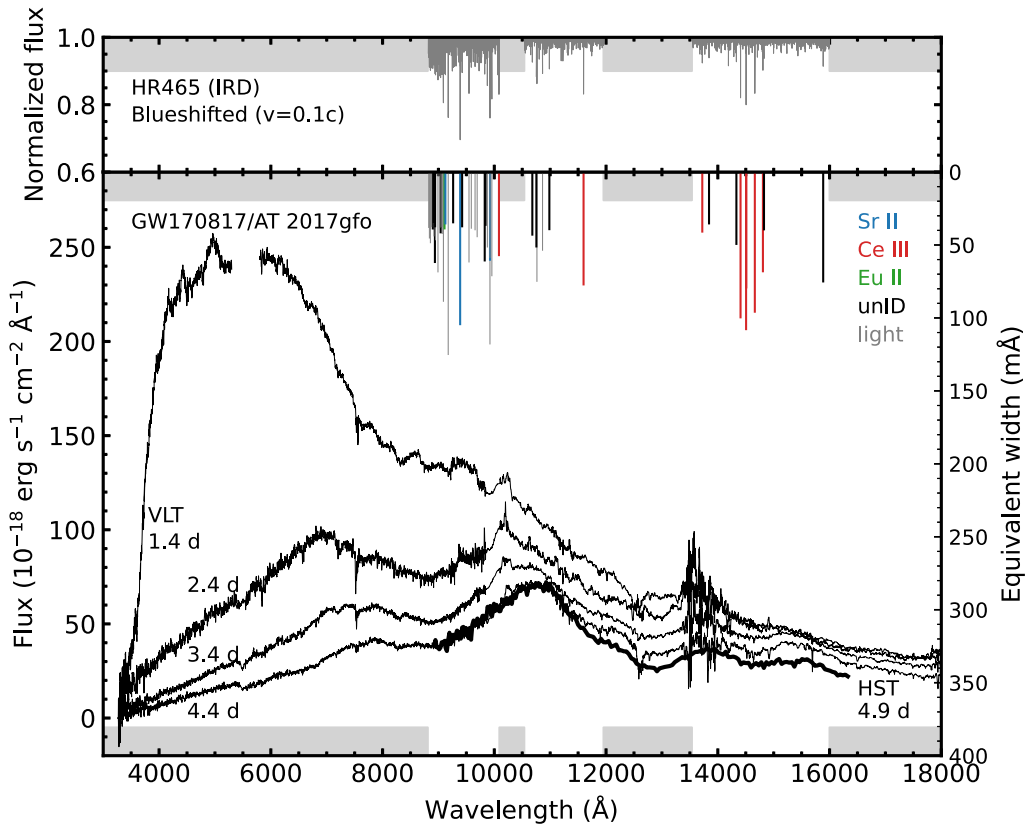


Figure 5. Top: the normalized spectrum of HR 465, blueshifted by $v = 0.1 c$. Bottom: spectra of AT 2017gfo taken with the Very Large Telescope (thin lines; Pian et al. 2017; Smartt et al. 2017) and Hubble Space Telescope (thick line; Tanvir et al. 2017). The vertical lines mark the EWs of strong transitions in HR 465, blueshifted by $v = 0.1 c$. The gray shaded region shows the wavelength range between the atmospheric windows for HR 465 (also blueshifted), where information of strong transitions are not available. The colors of the EWs are given according to the line identifications: Sr II (blue), Ce III (red), Eu II (green), unID (black), and elements lighter than Fe (gray).

not necessarily represent the relative line strengths in kilonovae.

The broad feature at 13000 \AA in the kilonova was identified as La III by Domoto et al. (2022). However, we could not test this identification with HR 465 because these lines are located in the wavelength range between the atmospheric windows at the rest wavelengths. To test this identification with stellar spectra, it is necessary to take high-resolution spectra between the J and H bands.

5. Concluding Remarks

We demonstrate that the spectra of chemically peculiar stars offer an excellent astrophysical laboratory to decode kilonova spectra. Thanks to the enhanced trans-iron abundances and similar ionization degrees, the absorption features in chemically peculiar stars can provide candidates for the strong transitions in kilonova spectra. This is particularly true for lanthanides: their abundances in chemically peculiar stars can be remarkably similar to those in kilonovae. By using an NIR spectrum of HR 465, we show that (i) the Ce III lines give the dominant contributions to the kilonova feature around 14500 \AA at early phases, and (ii) there are no other comparably strong transitions in this wavelength range even including unID lines. These facts support the Ce III identification by Domoto et al. (2022).

It should be noted that our analysis assumes LTE for ionization and excitation. In a kilonova, nonthermal ionization

can be important in particular at later phases due to the presence of fast electrons from radioactive decays. Under such conditions, lanthanides are expected to stay at singly ionized or doubly ionized states (Hotokezaka et al. 2021; Pognan et al. 2022). This may explain the presence of the broad absorption feature around 14500 \AA even at later phases: the ionization degrees do not significantly evolve with time, and the same Ce III lines can keep contributing to the spectra. To test this possibility, detailed calculations are required by taking nonthermal ionization into account. Also, both kilonovae and stellar atmospheres have density and temperature gradients. In particular, the density structure is shallower in a kilonova, and different regions may contribute to the spectrum. Thus, analysis with more realistic density structures is necessary to fully confirm the similarity between kilonovae and stellar atmospheres.

Another caveat is that the abundance ratios of HR 465 are not identical to those in the kilonova ejecta. While the lanthanide fractions are quite similar as shown in Figure 1 (top panel), elements with $Z = 30\text{--}50$ are less abundant in HR 465. Strong NIR transitions are expected to be dominated by lanthanides (and actinides) due to their low-lying, dense energy levels (Domoto et al. 2022). Thus, we consider that it is less likely that many lighter elements can contribute to the strong NIR transitions. Nevertheless, it is worth investigating the NIR transitions for various elements in actual stars by obtaining high-resolution NIR spectra for more chemically peculiar stars with different abundance enhancements as well as different

stellar types (temperature and density). Such data will provide us with clues to decode kilonova spectra with different abundances at various epochs.

Acknowledgments

This research was supported by JST FOREST Program (grant No. JPMJFR212Y), NIFS Collaborative Research Program (grant No. NIFS22KIIIF005), the JSPS Grant-in-Aid for Scientific Research (grant Nos. 18H05442, 19H00694, 20H00158, 20H05855, 21H04499, and 21H04997), and the Grant-in-Aid for JSPS Fellows (grant No. 22KJ0317). N.D. acknowledges support from Graduate Program on Physics for

the Universe (GP-PU) at Tohoku University. The pyfits and astropy are implemented into the software program that was used for the data reduction of IRD spectra. The pyfits and PyRAF are products of the STScI, which is operated by AURA for NASA.

Software: Astropy (Astropy Collaboration et al. [2013](#), [2018](#)).

Appendix

Figure 6 is an enlarged view of the entire NIR spectrum of HR 465 taken with Subaru/IRD. Gray shaded regions without line identification show the wavelength range with strong telluric absorption and artifacts in the telluric correction.

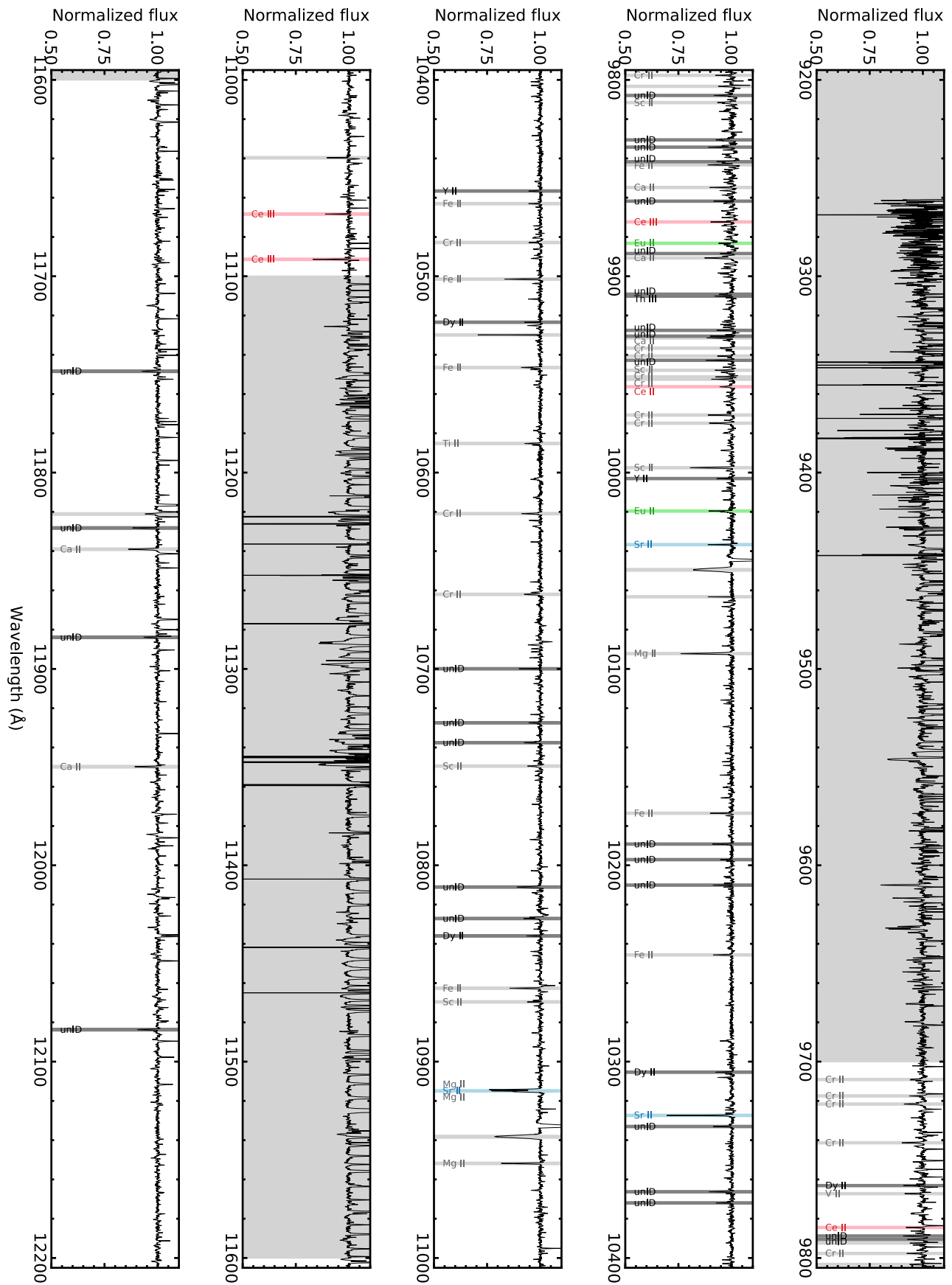


Figure 6. Normalized NIR spectrum of HR 465.

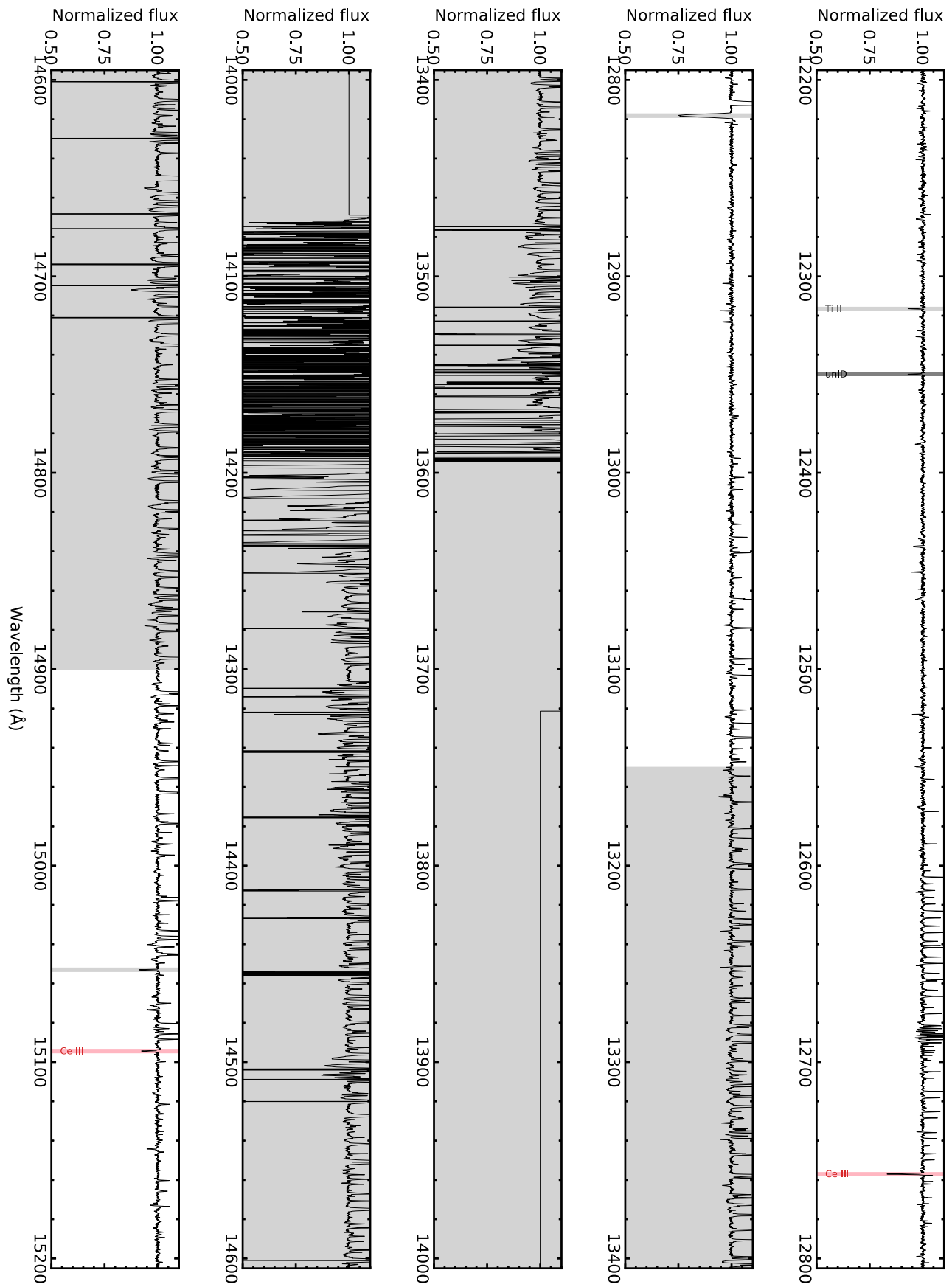


Figure 6. (Continued.)

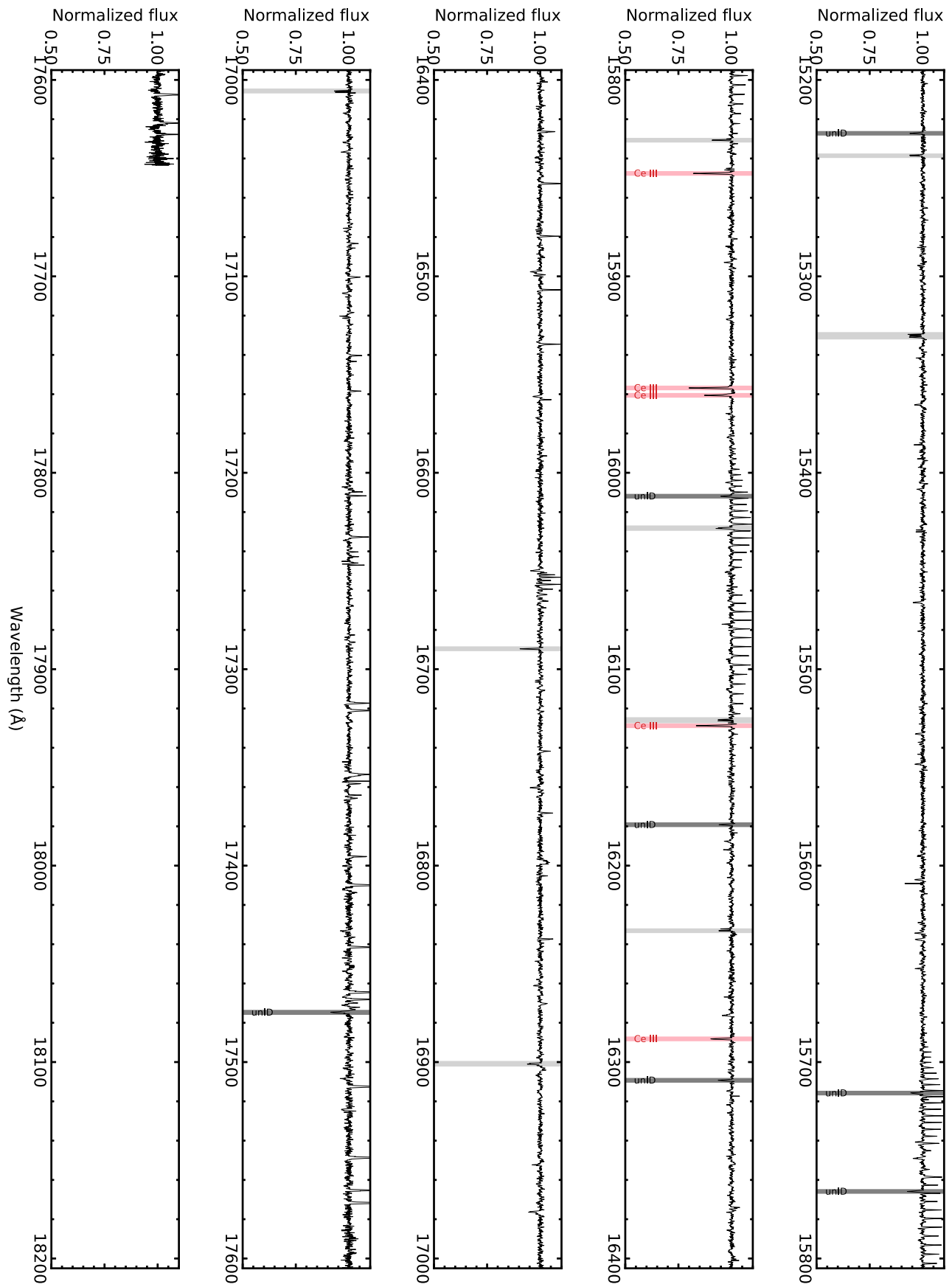











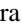






Figure 6. (Continued.)

ORCID iDs

Masaomi Tanaka  <https://orcid.org/0000-0001-8253-6850>
 Nanae Domoto  <https://orcid.org/0000-0002-7415-7954>
 Wako Aoki  <https://orcid.org/0000-0002-8975-6829>
 Miho N. Ishigaki  <https://orcid.org/0000-0003-4656-0241>
 Shinya Wanajo  <https://orcid.org/0000-0002-4759-7794>
 Kenta Hotokezaka  <https://orcid.org/0000-0002-2502-3730>
 Kyohei Kawaguchi  <https://orcid.org/0000-0003-4443-6984>
 Daiji Kato  <https://orcid.org/0000-0002-5302-073X>
 Jae-Joon Lee  <https://orcid.org/0000-0003-0894-7824>
 Ho-Gyu Lee  <https://orcid.org/0000-0002-3808-7143>
 Teruyuki Hirano  <https://orcid.org/0000-0003-3618-7535>
 Takayuki Kotani  <https://orcid.org/0000-0001-6181-3142>
 Masayuki Kuzuhara  <https://orcid.org/0000-0002-4677-9182>
 Jun Nishikawa  <https://orcid.org/0000-0001-9326-8134>
 Masashi Omiya  <https://orcid.org/0000-0002-5051-6027>
 Motohide Tamura  <https://orcid.org/0000-0002-6510-0681>

References

- Abbott, B. P., Abbott, R., Abbott, T. D., et al. 2017, *ApJL*, 848, L12
 Aller, M. F. 1972, *A&A*, 19, 248
 Aoki, W., Beers, T. C., Honda, S., et al. 2022, *PASJ*, 74, 273
 Asplund, M., Grevesse, N., Sauval, A. J., & Scott, P. 2009, *ARA&A*, 47, 481
 Astropy Collaboration, Price-Whelan, A. M., & Sipőcz, B. M. 2018, *AJ*, 156, 123
 Astropy Collaboration, Robitaille, T. P., & Tollerud, E. J. 2013, *A&A*, 558, A33
 Castelli, F., & Kurucz, R. L. 2003, in IAU Symp. 210, Modelling of Stellar Atmospheres, ed. N. Piskunov, W. W. Weiss, & D. F. Gray (San Francisco, CA: ASP), A20
 Chornock, R., Berger, E., Kasen, D., et al. 2017, *ApJL*, 848, L19
 Cowley, C. R., & Greenberg, M. 1987, *PASP*, 99, 1201
 Domoto, N., Tanaka, M., Kato, D., et al. 2022, *ApJ*, 939, 8
 Domoto, N., Tanaka, M., Wanajo, S., & Kawaguchi, K. 2021, *ApJ*, 913, 26
 Fontes, C. J., Fryer, C. L., Hungerford, A. L., Wollaeger, R. T., & Korobkin, O. 2020, *MNRAS*, 493, 4143
 Ghazaryan, S., Alecian, G., & Hakobyan, A. A. 2018, *MNRAS*, 480, 2953
 Gillanders, J. H., Smartt, S. J., Sim, S. A., Bauswein, A., & Goriely, S. 2022, *MNRAS*, 515, 631
 Honda, S., Aoki, W., Ishimaru, Y., Wanajo, S., & Ryan, S. G. 2006, *ApJ*, 643, 1180
 Hotokezaka, K., Tanaka, M., Kato, D., & Gaigalas, G. 2021, *MNRAS*, 506, 5863
 Kasen, D., Badnell, N. R., & Barnes, J. 2013, *ApJ*, 774, 25
 Kasen, D., Metzger, B., Barnes, J., Quataert, E., & Ramirez-Ruiz, E. 2017, *Natur*, 551, 80
 Kawaguchi, K., Shibata, M., & Tanaka, M. 2018, *ApJL*, 865, L21
 Kotani, T., Tamura, M., Nishikawa, J., et al. 2018, *Proc. SPIE*, 10702, 1070211
 Kupka, F., Piskunov, N., Ryabchikova, T. A., Stempels, H. C., & Weiss, W. W. 1999, *A&AS*, 138, 119
 Li, L.-X., & Paczyński, B. 1998, *ApJL*, 507, L59
 Metzger, B. D., Martínez-Pinedo, G., Darbha, S., et al. 2010, *MNRAS*, 406, 2650
 Michaud, G. 1970, *ApJ*, 160, 641
 Nielsen, K. E., Carpenter, K. G., Kober, G. V., & Wahlgren, G. M. 2020, *ApJ*, 899, 166
 Perego, A., Radice, D., & Bernuzzi, S. 2017, *ApJL*, 850, L37
 Perego, A., Vescovi, D., Fiore, A., et al. 2022, *ApJ*, 925, 22
 Pian, E., D'Avanzo, P., Benetti, S., et al. 2017, *Natur*, 551, 67
 Pognan, Q., Jerkstrand, A., & Gruner, J. 2022, *MNRAS*, 513, 5174
 Preston, G. W., & Wolff, S. C. 1970, *ApJ*, 160, 1071
 Pyper, D. M., & Adelman, S. J. 2017, *PASP*, 129, 104203
 Rice, J. B. 1988, *A&A*, 199, 299
 Rosswog, S., Sollerman, J., Feindt, U., et al. 2018, *A&A*, 615, A132
 Smartt, S. J., Chen, T.-W., Jerkstrand, A., et al. 2017, *Natur*, 551, 75
 Sneppen, A., Watson, D., Bauswein, A., et al. 2023, *Natur*, 614, 436
 Tamura, M., Suto, H., Nishikawa, J., et al. 2012, *Proc. SPIE*, 8446, 84461T
 Tanaka, M., & Hotokezaka, K. 2013, *ApJ*, 775, 113
 Tanaka, M., Kato, D., Gaigalas, G., & Kawaguchi, K. 2020, *MNRAS*, 496, 1369
 Tanaka, M., Utsumi, Y., Mazzali, P. A., et al. 2017, *PASJ*, 69, 102
 Tanvir, N. R., Levan, A. J., González-Fernández, C., et al. 2017, *ApJL*, 848, L27
 Tarumi, Y., Hotokezaka, K., Domoto, N., & Tanaka, M. 2023, arXiv:2302.13061
 Wanajo, S. 2018, *ApJ*, 868, 65
 Watson, D., Hansen, C. J., Selsing, J., et al. 2019, *Natur*, 574, 497